Journal of Marine Research, 66, 413–440, 2008

Journal of
MARINE RESEARCH

Volume 66, Number 4

Evaluating salt-fingering theories

by R. Inoue[1], E. Kunze[2,3], L. St. Laurent[4], R. W. Schmitt[5] and J. M. Toole[5]

ABSTRACT

The NATRE fine- and microstructure data set is revisited to test salt-finger amplitude theories. Dependences of the mixing efficiency Γ, microscale buoyancy Reynolds number Re and thermal Cox number Cx_T on 5-m density ratio R_ρ and gradient Richardson number Ri are examined. The observed mixing efficiency is too high to be explained by linear fastest-growing fingers but can be reproduced by wavenumbers 0.5-0.9 times lower than the fastest-growing wavenumber. Constraining these fingers with a hybrid wave/finger Froude number or a finger Reynolds number cannot reproduce the observed trends with R_ρ or Ri, respectively. This suggests that background shear has no influence on finger amplitudes. Constraining average amplitudes of these lower-wavenumber fingers with finger Richardson number $Ri_f \sim 0.2$ reproduces the observed dependence of Re and Cx_T on density ratio R_ρ and Ri at all but the lowest observed density ratio ($R_\rho = 1.3$). Separately relaxing the assumptions of viscous control, dominance of a single mode and tall narrow fingers does not explain the difference between theory and data at low R_ρ for a critical $Ri_f \sim 0.2$.

1. Introduction

Salt-fingering is a double-diffusive instability that arises when an unstable vertical salinity gradient is stabilized by temperature. It is strongest when the salinity gradient almost compensates the temperature gradient. Fingering-favorable conditions are found in the subtropical Atlantic and Indian pycnoclines (Schmitt, 1981, 2003; You, 2002), below salt tongues originating from the Mediterranean and Red seas (e.g.,

1. Applied Physics Laboratory, University of Washington, 1013 NE 40th Street, Seattle, Washington, 98105-6698, U.S.A.
2. School of Earth and Ocean Sciences, University of Victoria, Victoria, BC, V8W 3P6, Canada.
3. Corresponding author. ***email: kunze@uvic.ca***
4. Department of Oceanography, Florida State University, Tallahassee, Florida, 32306, USA.
5. Woods Hole Oceanographic Institution, Woods Hole, Massachusetts, 02543, U.S.A.

Williams, 1974; Magnell, 1976), and in double-diffusive intrusions that form at density-compensated water-mass fronts (Toole and Georgi, 1981; Ruddick and Richards, 2003). Of principal interest to the general oceanographic community is their heat- and salt-fluxes as these can lead to water-mass modification and lower the available potential energy of the water column. While theory for the initial growth of these instabilities is well-established (Stern, 1969; Schmitt, 1979a; Kunze, 1987), what sets their amplitudes in the ocean is far less certain because the mechanisms that arrest finger growth are nonlinear and unknown (Kunze, 2003). In the ocean, there are also potentially confounding influences from turbulence (Linden, 1971; Taylor, 1991; Wells and Griffiths, 2002) and internal wave shearing (Linden, 1974; Kunze *et al.*, 1987; Kunze, 1990, 1994).

The importance of quantifying these fluxes was recognized early. Two-layer laboratory experiments (Turner, 1967; Linden, 1973; Schmitt, 1979b; McDougall and Taylor, 1984; Taylor and Bucens, 1989) suggested $\Delta S^{4/3}$ flux laws where ΔS is the salinity difference between the layers. Applying the 4/3 flux laws in a thermohaline staircase east of Barbados, Lambert and Sturges (1977) inferred a salt eddy diffusivity of 5×10^{-4} m^2 s^{-1}. But these flux laws overestimate inferred fluxes in the permanent thermohaline staircase east of Barbados by an order of magnitude (Gregg and Sanford, 1987; Lueck, 1987; Fleury and Lueck, 1991), a result confirmed by a tracer-release experiment (Schmitt *et al.*, 2005). Kunze (1987) suggested that this was because the staircase interfaces are much thicker than those in laboratory experiments. Stern (1969) put forward an ad-hoc nondimensional constraint $\langle w'b' \rangle / (\nu N^2) \sim \mathrm{O}(1)$ that came to be known as the Stern number, where ν is molecular viscosity and N the buoyancy frequency. Kunze (1987) showed that the Stern number was equivalent to an inverse finger Richardson number $Ri_f^{-1} = (\nabla w)^2 / N^2$, provided that vertical acceleration can be ignored ($\nu \nabla^2 \gg \partial / \partial t$), and that $Ri_f = 0.25$ was able to reproduce observed staircase fluxes when applied to the maximum amplitude of growing fingers. This constraint also seemed consistent with vertical erosion of a Meddy's core (Hebert, 1988) but when applied to average finger amplitude. Based on measurements in a continuously stratified fingering-favorable region of the eastern North Atlantic, St. Laurent and Schmitt (1999) suggest that the vertical diffusivity of salt associated with low density ratio R_ρ and high Richardson number Ri is an order of magnitude higher than predicted by finger Richardson number constraint $Ri_f = 0.25$ applied to maximum finger amplitude. Their diffusivity decreases with increasing R_ρ in contrast to the predicted trend for fastest-growing fingers. Observed signals are associated with mixing efficiencies $\Gamma = (\bar{N}^2 / 2\varepsilon)(\chi_T / \bar{\theta}_z^2) \approx 0.4 - 0.8$, much higher than could be explained by the $\Gamma \leq 0.2$ of isotropic turbulence (Osborn, 1980; Oakey, 1982) and more consistent with those predicted for salt fingers (McDougall, 1988; Hamilton *et al.*, 1989, 1993), where ε is turbulent kinetic energy dissipation rate, χ_T thermal dissipation rate, $\bar{\theta}_z$ background vertical potential temperature gradient and $\bar{N}^2$ background buoyancy frequency squared.

Numerical simulations of salt-finger convection are challenging because of the large range of length-scales that must be included for realistic Prandtl number $\nu/\kappa_T = 7$ and diffusivity ratio $\kappa_S/\kappa_T = 0.01$ (e.g., Piacsek and Toomre, 1980; Yoshida and Nagashima, 2003). As a result, modelers often resort to two-dimensional simulations, even though it is known that stability problems are inherently different in 2- and 3-D (e.g., Winters and Riley, 1992; Radko and Stern, 1999), or use higher Lewis numbers. To reproduce the $\Delta S^{4/3}$ flux laws found in laboratory experiments, layered systems have been examined in 2-D (Whitfield *et al.*, 1989; Piacsek *et al.*, 1988; Shen, 1989, 1993; Shen and Veronis, 1991, 1997; Özgökmen and Esenkov, 1998) and 3-D (Radko and Stern, 2000). More relevant to most of the fingering-favorable parts of the ocean, including the NATRE measurements, are simulations with continuous vertical gradients which have also been conducted both in 2-D (Shen, 1995; Özgökmen *et al.*, 1998; Stern and Radko, 1998; Merryfield, 2000; Stern *et al.*, 2001; Stern and Simeonov, 2002; Radko, 2003, 2005) and 3-D (Radko and Stern, 1999; Stern *et al.*, 2001; Stern and Simeonov, 2004; Stern and Simeonov, 2005). Shen (1995) suggests that equilibrium arises from detachment of buoyant blobs at finger tips. His simulations produced fluxes increasing with the mean vertical temperature or salinity gradients at fixed density ratio R_ρ and decreasing with R_ρ. The relation between fluxes from 2-D and 3-D simulations was explored by Stern *et al.* (2001) but needs further investigation due to their limited computer resources. Stern and Radko (1998), Radko and Stern (1999) and Stern and Simeonov (2004) suggest that amplitude equilibration is achieved via nonlinear triad interactions in the sugar-salt system. Alternatively, Stern and Simeonov (2005) proposed a secondary instability mode which accompanies fastest-growing fingers in the heat-salt system, then parameterized fluxes using an eddy length due to fingers. While numerical simulations have made great strides in recent years, because of the need to resolve a broad range of scales and influences, these still have not converged and further research is needed.

In this paper, we test salt-fingering theories (Section 2) to explore which proposed constraints might set finger amplitudes in the ocean. We revisit the St. Laurent and Schmitt (1999) data set in Section 3. In Section 4, we show that fastest-growing fingers (Stern, 1960; Schmitt, 1979a; Kunze, 1987) cannot explain the observed decreasing (increasing) trend of Γ with R_ρ (Ri). Wavenumbers which reproduce the observed trends in Γ are obtained diagnostically. These wavenumbers are lower (larger wavelengths) than fastest growing. Observed microscale buoyancy Reynolds number Re and Cox number Cx_T are compared to values predicted from linear theory constrained by various nondimensional constraints including finger Richardson number Ri_f (Kunze, 1987), hybrid wave/finger Froude number $Fr_{w/f}$ (Kunze, 1994) and finger Reynolds number Re_f. We also compare the data with a recent parameterization of Cx_T from numerical modeling (Stern *et al.*, 2001). In Section 5, the assumptions of viscous damping ($\nu\nabla^2 \gg \partial/\partial t$), single wavenumber and tall narrow fingers ($\nabla^2 \approx \partial^2/\partial x^2 + \partial^2/\partial y^2$) used in the standard linear finger model are relaxed to see how they affect the discrepancy between data and theoretical predictions. The single-wavenumber assumption is addressed by using a salt-finger wavenumber spectral model (Schmitt, 1979a; Shen and Schmitt, 1995) to determine contributions from salt-

fingering wavebands other than a single wavenumber. The results are summarized and unaddressed issues discussed in Section 6.

2. Salt-fingering theory

The governing equations for linear salt fingers are

$$\begin{aligned} \frac{\partial w}{\partial t} - \nu\nabla^2 w &= g(\alpha\delta\theta - \beta\delta S) \\ \frac{\partial(\delta\theta)}{\partial t} - \kappa_T\nabla^2(\delta\theta) + w\theta_z &= 0 \\ \frac{\partial(\delta S)}{\partial t} - \kappa_S\nabla^2(\delta S) + wS_z &= 0 \end{aligned} \tag{1}$$

(Stern, 1960), where w is the vertical velocity due to salt-fingering, g gravitational acceleration, $\delta\theta$ and δS temperature and salinity contrasts between fingers, α the thermal expansion coefficient, β the haline contract coefficient, θ_z and S_z vertical temperature and salinity gradients within the fingers, ν molecular viscosity, κ_T molecular heat diffusivity and κ_S molecular salt diffusivity with $\nu \gg \kappa_T \gg \kappa_S$.

Solutions to these equations commonly rely on three assumptions (e.g., Stern, 1960; Schmitt, 1979a; Kunze, 1987; Smyth and Kimura, 2007):

(i) neglect of the acceleration term $\partial w/\partial t$ in the vertical momentum conservation equation (viscous control),
(ii) tall narrow fingers for which $\nabla^2 \approx \partial^2/\partial x^2 + \partial^2/\partial y^2$, and
(iii) sinusoidal horizontal finger structure $\sin(kx)$ where k is horizontal wavenumber.

With these assumptions, the growth rate σ can be written

$$\sigma(k) \cong \frac{1}{4}\left[\kappa_T k^2 + \frac{g\beta\bar{S}_z(R_\rho - 1)}{\nu k^2}\right] \cdot \left\{\sqrt{1 + \frac{4[(\kappa_T - R_\rho\kappa_S)g\beta\bar{S}_z - \nu\kappa_T\kappa_S k^4]}{\nu\left[\kappa_T k^2 + \frac{g\beta\bar{S}_z(R_\rho - 1)}{\nu k^2}\right]^2}} - 1\right\} \tag{2}$$

(Kunze, 1987) where $\bar{S}_z$ and $R_\rho = \alpha\bar{\theta}_z/(\beta\bar{S}_z)$ are the background salinity gradient and density ratio, respectively. The growth rate for fastest-growing fingers is

$$\sigma_{FG} \cong \frac{1}{2}\sqrt{\frac{\kappa_T g\beta\bar{S}_z}{\nu}}\,(\sqrt{R_\rho} - \sqrt{R_\rho - 1}) \tag{3}$$

with fastest-growing wavenumber

$$k_{FG} \cong \left(\frac{g\beta\bar{S}_z(R_\rho - 1)}{\nu\kappa_T}\right)^{1/4} \tag{4}$$

(Stern, 1975; Schmitt, 1979a; Kunze, 1987).

To compare theory with microstructure observations, we use the nondimensional microstructure buoyancy Reynolds number Re (Gargett, 1988), thermal Cox number Cx_T (Osborn and Cox, 1972) and mixing efficiency Γ. Observed parameters are estimated as

$$\begin{aligned} Re_{obs} &= \frac{\varepsilon_{obs}}{\nu \bar{N}^2} = \frac{15}{2}\frac{\langle u_z^2 \rangle}{\bar{N}^2}, \\ Cx_{T\,obs} &= \frac{\chi_{T\,obs}}{2\kappa_T \bar{\theta}_z^2} = \frac{3\langle \delta\theta_z^2 \rangle}{\bar{\theta}_z^2}, \\ \Gamma_{obs} &= \frac{\bar{N}^2 \chi_{T\,obs}}{2\bar{\theta}_z^2 \varepsilon_{obs}} = \frac{\kappa_T}{\nu}\frac{Cx_{T\,obs}}{\mathrm{Re}_{obs}} = \frac{2}{5}\frac{\kappa_T}{\nu}\frac{\bar{N}^2 \langle \delta\theta_z^2 \rangle}{\bar{\theta}_z^2 \langle u_z^2 \rangle}, \end{aligned} \tag{5}$$

where ε is the dissipation rate of kinetic energy due to molecular viscosity υ, and χ_T is the dissipation rate of temperature variance due to thermal molecular diffusivity κ_T. The factor of 2 in the denominator of Cx_T arises from the definition of χ_{Tobs} (Osborn and Cox, 1972). Theoretical finger Reynolds number Re, thermal Cox number Cx_T and mixing efficiency Γ are estimated as

$$\begin{aligned} Re_{theo} &= \frac{\varepsilon_{theo}}{\nu \bar{N}^2} = \frac{w_x^2}{\bar{N}^2} = \frac{k^2 w^2}{\bar{N}^2} = \frac{C_w k^2 \sigma(k)^2 \langle h^2 \rangle}{4\bar{N}^2}, \\ Cx_{T\,theo} &= \frac{\chi_{T\,theo}}{\kappa_T \bar{\theta}_z^2} = \frac{k^2 \delta\theta^2}{\bar{\theta}_z^2} = \frac{C_T k^2 \sigma(k)^2 \langle h^2 \rangle}{4[2\sigma(k) + \kappa_T k^2]^2}, \\ \Gamma_{theo} &= \frac{\bar{N}^2 \chi_{T\,theo}}{2\bar{\theta}_z^2 \varepsilon_{theo}} = \frac{\kappa_T}{\nu}\frac{Cx_{T\,theo}}{\mathrm{Re}_{theo}} = \frac{\kappa_T}{\nu}\frac{\bar{N}^2 \delta\theta_x^2}{\bar{\theta}_z^2 w_x^2} = \frac{C_T}{C_w}\frac{\kappa_T}{\nu}\frac{\bar{N}^2}{[2\sigma(k) + \kappa_T k^2]^2}, \end{aligned} \tag{6}$$

using $w = \partial h/\partial t = \sigma h/2$ and the nondimensional temperature difference between up- and downgoing fingers $-\dfrac{2\delta\theta}{\bar{\theta}_z h} = \dfrac{\sigma}{2\sigma + \kappa_T k^2}$ (Kunze, 1987), where h is the finger height. Depending on the horizontal planform, horizontal averaging variance coefficients $C_w = C_T = \int_0^{\lambda} \sin^2(kx)dx = 1/2$ for sinusoidal sheet planform fingers. The $\langle \cdot \rangle$ average in (6) will denote either an ensemble-average of statistically steady fingers or a time-average of growing fingers over time interval $t_{\max}$ from their inception to when the finger amplitude h exceeds a threshold constraint (discussed next). We will make use of the fact that mixing efficiency Γ_{theo} is independent of finger amplitude h to show that observed mixing efficiency cannot be explained by fastest-growing fingers regardless of amplitude.

Clearly, (5) and (6) are not the same. First, the observed Γ (5) has a factor of 2/5 in it from the assumption of isotropy while fingers are not isotropic. Second, the observed Γ is based on *vertical* gradients of *horizontal* velocities while the finger Γ is based on *horizontal* gradients of *vertical* finger velocities. In contrast to laboratory experiments at high density ratios which find tall well-ordered vertical fingers, numerical simulations and laboratory experiments at low density ratios observe disordered, jumbled finger fields with aspect ratios O(1) (e.g., Merryfield, 2000). Thus, the assumption of isotropy in the

observations may be appropriate. But this calls into question the tall-narrow finger assumption in the theory (which is addressed in Section 5) and possibly calls for adjustment of the theoretical relations. Following St. Laurent and Schmitt (1999), we will take the observed (5) and theoretical (6) parameters to be equivalent for comparison purposes but urge caution in the interpretation and will return to this issue in the Discussion (Section 6).

For fastest-growing fingers (3) and (4), (6) becomes

$$\begin{aligned} Re_{FG} &= \frac{C_w k^2 \sigma^2 h^2}{4\bar{N}^2} = \frac{\sqrt{\kappa_T}\,\bar{N}(\sqrt{R_\rho} - \sqrt{R_\rho - 1})^2 h^2}{32\nu^{3/2}(R_\rho - 1)}, \\ Cx_{T\,FG} &= \frac{C_T k^2 \sigma^2 h^2}{4(2\sigma + \kappa_T k^2)^2} = \frac{\bar{N}(\sqrt{R_\rho} - \sqrt{R_\rho - 1})^2 h^2}{32\sqrt{\nu\kappa_T}\,R_\rho}, \\ \Gamma_{FG} &= \frac{C_T}{C_w}\frac{\kappa_T}{\nu}\frac{\bar{N}^2}{(2\sigma + \kappa_T k^2)^2} = \frac{R_\rho - 1}{R_\rho}. \end{aligned} \tag{7}$$

The mixing efficiency Γ differs from the relation found by Hamilton *et al.* (1989)

$$\Gamma_{FG} = \frac{R_\rho - 1}{R_\rho}\frac{R_F}{1 - R_F} = \sqrt{\frac{R_\rho - 1}{R_\rho}}$$

for fastest-growing finger flux ratio $R_F = \sqrt{R_\rho}\,(\sqrt{R_\rho} - \sqrt{R_\rho - 1})$ (Stern, 1975) because their relation is derived from steady turbulent kinetic energy and temperature variance conservation in analogy to the steady turbulent balances, while fastest-growing fingers are unsteady.

Without any constraint, finger height h will grow indefinitely to produce unrealistically unbounded vertical fluxes of heat and salt. This suggests that there is a mechanism which disrupts growth of fingers in the ocean. In this study, we focus on three ad-hoc constraints (Stern, 1969; Kunze, 1987, 1994, 2003) for nonlinear breakdown of finger growth by secondary instability. We caution that the connection between any of these constraints and secondary instability of fingers is not well established. As described in the introduction, numerical simulations suggest that finger amplitude may be controlled by the shedding of blobs from growing finger tips or secondary instability associated with nonlinear triad interactions:

1. *Finger Richardson number* assumes salt-finger growth is disrupted by shear between fingers overcoming the vertical stratification,

$$Ri_f = \frac{N_f^2}{(\nabla_h w)^2} = \frac{4N_f^2}{C_w k^2 \sigma^2 h^2}\left(= \frac{N_f^2}{\bar{N}^2 Re_{theo}}\right), \tag{8}$$

where N_f is the horizontally-averaged finger-modified buoyancy frequency

$$N_f^2 \cong \frac{g\beta\bar{S}_z}{2}\sqrt{R_\rho - 1}\,(\sqrt{R_\rho} + \sqrt{R_\rho - 1}) \tag{9}$$

(Kunze, 1987). For constraint (8), finger height

$$h = \frac{2N_f}{\sqrt{C_w Ri_f}\,\sigma k}. \tag{10}$$

The presence of the horizontal averaging coefficient C_w signifies that we are constraining the variance of Ri_f, not maximal values. If maximal values were constrained, the resulting h would be smaller by a factor of $\sqrt{2}$. For square planform fingers $\sin(kx)\sin(ky)$, h would be larger by $\sqrt{2}$. Note that Ri_f and Re_{theo} (6) are simply related (8). When viscous damping dominates, (10) is identical to that from the Stern number (Stern, 1969). Holyer (1984) found that fingers are unstable to secondary instability regardless of Ri_f, suggesting that the breakdown of fingers does not have the same dynamics as shear instability. In sugar-salt lab studies, the Stern number ranges from 0.1-0.001 (Lambert and Demenkow, 1971; Griffiths and Ruddick, 1980), suggesting that Ri_f approaches infinity as the Prandtl number becomes very large (Radko and Stern 2000).

2. *Hybrid wave/finger Froude number* involves orthogonal components of finger shear w_y and background shear U_z

$$Fr_{w/f} = \frac{|U_z w_y|}{N_f^2} \tag{11}$$

(Kunze, 1994). This assumes that fingers form sheets aligned with the shear (Linden, 1974). Resulting finger height

$$h = \frac{2Fr_{w/f}N_f^2}{\sqrt{C_w}\,U_z\sigma k}. \tag{12}$$

We use the finger-modified stratification N_f^2 (9) felt by the fingers rather than the background stratification $\bar{N}^2 = g\beta\bar{S}_z(R_\rho - 1)$ used in Kunze (1994). However, the finescale shear $U_z = \sqrt{\bar{N}^2/Ri}$ is defined using the background stratification.

3. *Finger Reynolds number* describes when nonlinear salt-fingering inertia exceeds viscous damping

$$Re_f = \frac{|w\nabla w|}{\nu\nabla^2 w} = \frac{\sqrt{C_w}\,kw}{\nu k^2} = \frac{\sqrt{C_w}\,\sigma h}{2\nu k}, \tag{13}$$

for which finger height

$$h = \frac{2\,Re_f \nu k}{\sqrt{C_w}\,\sigma}. \tag{14}$$

This constraint has not been used in previous studies although Stern (1969) noted that it was equivalent to the Stern number. Note that the finger Reynolds number *constraint* Re_f (13) differs in form from the theoretical finger Reynolds numbers Re_{theo} (6) that will be compared with the observed microstructure Reynolds number (5).

The thresholds are applied both (i) assuming the constraint applies to an ensemble-average finger height $\langle h \rangle$ in a statistically stationary finger field, and (ii) assuming fingers grow from small perturbations $h_0 = \lambda = 2\pi/k$ to be disrupted at a maximum finger height $h = h_{\max}$ set by the given constraint, then repeat this cycle. Case (i) might apply if finger amplitudes are limited by shedding elongated blobs from their tips. In this case, Re and Cx_T are obtained directly from (6) and will be denoted $\langle \rangle_e$. In case (ii), maximum Re and Cx_T obtained from (6) are normalized assuming exponential growth by

$$2\sigma t_{\max} = 2 \ln \left(\frac{h_{\max}}{h_0} \right) = 2 \ln \left(\frac{k h_{\max}}{2\pi} \right) \tag{15}$$

(Kunze, 1987). The resulting time-averages are denoted $\langle \rangle_m$. Average Re and Cx_T for case (ii) found to be independent of h_0 for $h_0 = 1/k - 2\pi/k$ because finger height grows to be much larger than h_0 for $R_\rho = 1.3$-2.

3. Observations

Fine- and microstructure data were collected with the High-Resolution Profiler (Schmitt *et al.*, 1988) during the North Atlantic Tracer-Release Experiment (NATRE, Ledwell *et al.*, 1993). The bulk of the fingering-favorable data comes from isopycnals lighter than those where warm salty Mediterranean Salt Tongue and cool fresh Labrador Sea water-masses are stirred down to finescale filaments and interleave (St. Laurent and Schmitt, 1999; Ferrari and Polzin, 2005). These shallower density surfaces are characterized by density ratios $R_\rho < 2$ while those in the denser interleaving water have $R_\rho > 2$. The High-Resolution Profiler is equipped with CTD sensors and an acoustic velocimeter as well as microscale shear and temperature probes. We use data previously processed and interpreted by St. Laurent and Schmitt (1999), namely 121,441 samples of finescale stratification $\bar{N}^2$, potential temperature gradient $\bar{\theta}_z$, density ratio $R_\rho = \alpha \bar{\theta}_z / (\beta \bar{S}_z)$, gradient Richardson number $Ri = \bar{N}^2 / (U_z^2 + V_z^2)$, as well as microscale kinetic energy turbulent dissipation rate ε and temperature variance dissipation rate χ_T [$> 10^{-9}$ °C^2 s^{-1}, St. Laurent and Schmitt, 1999]. Microscale quantities have been binned in 0.5-m intervals while finescale quantities are based on 5-m fits centered on the microscale bins.

St. Laurent and Schmitt (1999) distinguished salt fingering from turbulence using observed mixing efficiencies in 5-m density ratio R_ρ and Richardson number Ri spaces, finding that salt-fingering signals were most consistently found for $1 < R_\rho < 2$ and $Ri > 1$. Restricting the data set to these R_ρ and Ri ranges reduces the number of bins to 33,661 (28%). After further eliminating data suspected by being noisy following Schmitt *et al.* (1988) and Toole *et al.* (1994) (Table 1), the number of bins is reduced to 26,153 (22%).

Histograms of ε peak around 10^{-10} W kg^{-1} but the criteria $1 < R_\rho < 2$ and $Ri > 1$ still allow ε as high as 10^{-8} W kg^{-1} (Fig. 1a). Since our study focuses on salt-fingering signals without contributions from turbulence, we further restrict the buoyancy Reynolds number $Re = \varepsilon/(\nu \bar{N}^2) < 20$ to exclude possible turbulent signals. This restriction is consistent with

Table 1. Observed quantities and noise levels.

Observed quantities	Noise level
$\bar{\theta}_z$	$2.0 \times 1.4 \times 10^{-4}/5.0$ °C m^{-1}
$\bar{S}_z$	$2.0 \times 10^{-3}/5.0$ psu m^{-1}
$\bar{N}^2$	3.0×10^{-6} s^{-2}
U_z	$2.0 \times 2^{1/2} \times 6.5 \times 10^{-4}/5.0$ s^{-1}
ε	5.3×10^{-11} W kg^{-1}
χ_T	10^{-9} °C^2 s^{-1}

past observations in C-SALT (Gregg, 1988) and the criterion for buoyancy-restricted turbulence (Stillinger *et al.*, 1983; Itsweire *et al.*, 1986). This criterion reduces the number of bins under consideration to 18,389 (15%). We caution that the resulting subset could still include low-Reynolds-number turbulence which should be characterized by moderate ε, low Cx_T and low Γ (Gargett, 1988; Ruddick *et al.*, 1997).

In this study, a less restrictive criterion $Ri > 0.25$ rather than $Ri > 1.0$ (St. Laurent and Schmitt, 1999) is used because we found that this criterion produces the same trends (Fig. 1b). This raises the number of bins available for analysis to 27,712 (23%).

Nondimensional 5-m density ratio R_ρ and Richardson number Ri define our background parameter space. R_ρ-binned mean Ri lies between 3 and 7 with larger values for $R_\rho > 1.4$, while Ri-binned mean R_ρ is nearly constant around 1.65 (Fig. 2). R_ρ-binned mean $\bar{\theta}_z$ and $\bar{N}^2$ are increasing functions for $R_\rho < 1.5$, and decreasing functions for $R_\rho > 1.5$ (Fig. 3). The 5-m $\bar{\theta}_z$ and $\bar{N}^2$ become small as R_ρ approaches one as one might expect. Ri-binned mean $\bar{\theta}_z$ and $\bar{N}^2$ are both increasing functions, suggesting that mean stratification contributes to Ri variability.

Using the bootstrap method (Efron and Gong, 1983), the 5-m scale variables are sorted in R_ρ or Ri spaces which are subdivided by 2000 samples per bin, yielding 13 bins. 2000 random samples with replacement are selected from each bin to obtain bin averages. The mean and 95% confidence limits of 1000 such averages are then estimated.

4. Comparison with data

a. Mixing efficiencies Γ

To test the validity of fastest-growing fingers often assumed, we compare the observed and theoretical mixing efficiencies Γ (5) and (6). Observed Γ obtained from our criteria is higher than that obtained by St. Laurent and Schmitt (1999) because of our restriction $Re < 20$. But, as found by St. Laurent and Schmitt, it is a weakly decreasing function of R_ρ (Fig. 4a) since the decreasing trend is stronger in Cx_T than that in Re (see Figs. 6-7). The approximate dependence of the observed mixing efficiency to density ratio is $\Gamma \sim \dfrac{\sqrt{R_\rho}}{2\sqrt{R_\rho - 1}}$. Mixing efficiency Γ is an increasing function of finescale Richardson number Ri (Fig. 4b) because Re has a decreasing trend. Low-Reynolds-number turbulence

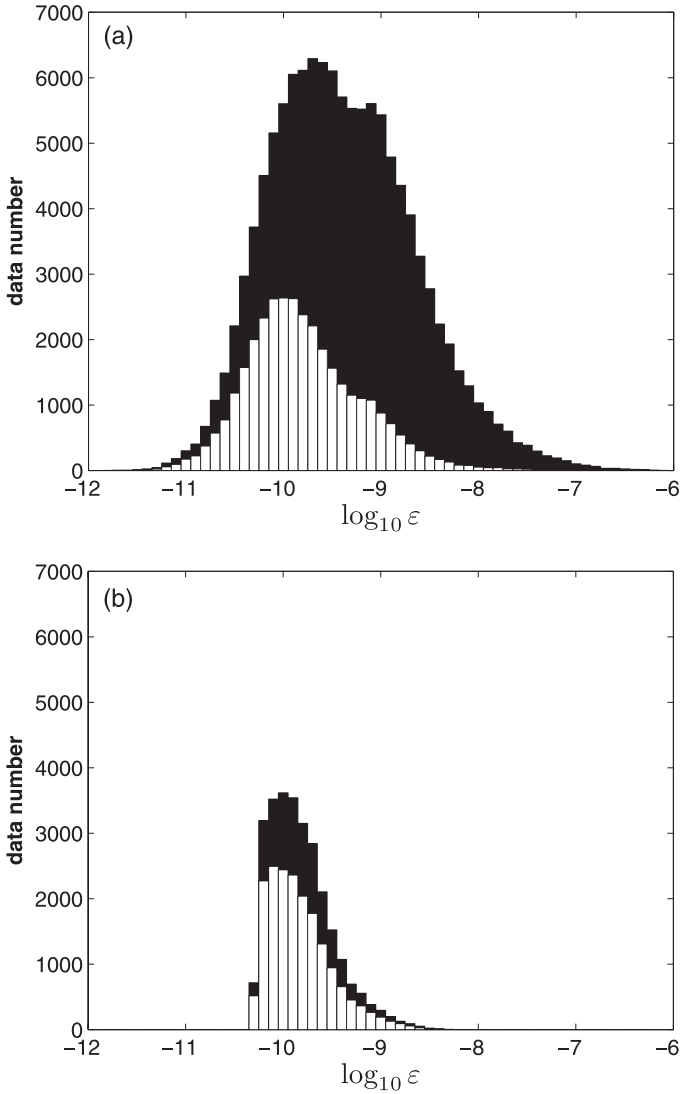

Figure 1. Histograms of ε. In (a), black bars show all the data, white bars are restricted to $Ri > 1.0$ and $1 < R_\rho < 2$. In (b), black bars exclude noisy data as well as restrictions $Ri > 0.25$, $1 < R_\rho < 2$ and $Re < 20$, white bars restrict $Ri > 1.0$ rather than $Ri > 0.25$.

may contribute some of the variance at low *Ri*. Consistent with this, we see enhanced *Re* but not Cx_T at low *Ri*.

The increasing theoretical trend of Γ with R_ρ for fastest-growing fingers (7) is not reproduced observationally. Moreover, the fastest-growing Γ underestimates the observed mixing efficiencies. Since theoretical Γ is independent of finger amplitude, this cannot be explained by any of

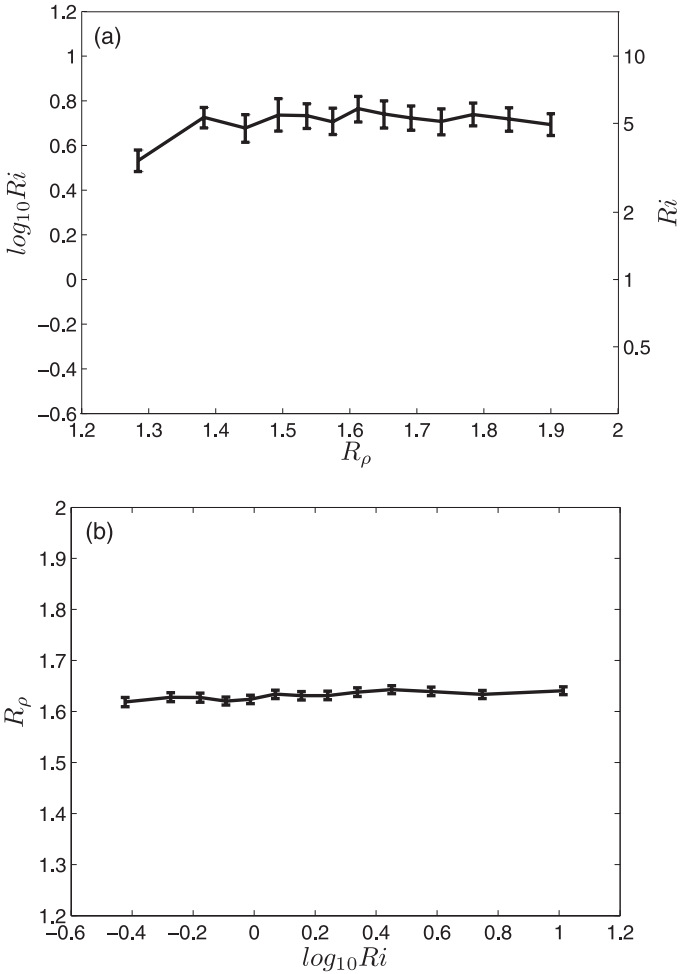

Figure 2. Average dependence of 5-m (a) Richardson number *Ri* on 5-m density ratio R_ρ and (b) density ratio R_ρ on Richardson number *Ri*. Vertical bars denote 95% confidence limits. Axes ranges were chosen to correspond between the two panels.

the amplitude constraints. However, it is explicable by fingers with lower than fastest-growing wavenumber (6). Figure 5 shows the best-fit wavenumbers *k* that can reproduce the observed trend of Γ with density ratio. These range from roughly $0.5k_{FG}$ at $R_\rho = 1.3$ to $0.9k_{FG}$ at $R_\rho = 2$ and can be expressed as a quadratic function of R_ρ as $k = -120R_\rho{}^2 + 460R_\rho - 334$. This form is used to test each finger constraint as a function of density ratio.

b. Reynolds (Re) and thermal Cox (Cx_T) numbers

Observed buoyancy Reynolds number *Re* and thermal Cox numbers Cx_T decrease weakly both with increasing R_ρ (Figs. 6-7). Observed *Re* decreases weakly with *Ri* (Fig. 6)

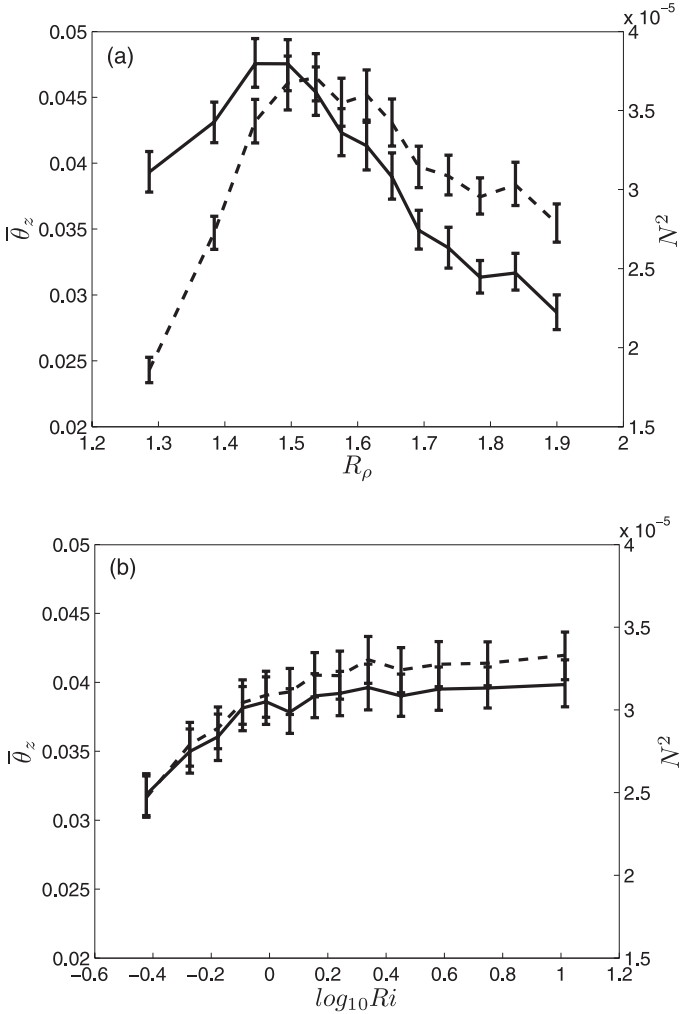

Figure 3. Average dependence of 5-m temperature gradient $\bar{\theta}_z$ (solid curve) and buoyancy frequency $\bar{N}^2$ (dashed curve) on (a) 5-m R_ρ and on (b) 5-m *Ri*. Vertical bars denote 95% confidence limits.

while Cx_T shows little dependence on *Ri* (Fig. 7). The best-fit values of the constraints Ri_f, $Fr_{w/f}$ and Re_f that reproduce the average *Re* and Cx_T are summarized in Table 2 assuming the constraints are applied to best-fit wavenumbers (Fig. 5) for both ensemble $\langle\rangle_e$ and maximum amplitude of growing fingers $\langle\rangle_m$. Dynamically plausible values ($Ri_f \sim 0.25$, $Fr_{w/f} \sim 2.0$, $Re_f \sim 1.0$) are shown in bold. We emphasize that the constraints are applied to the total averages so that model functional dependences on R_ρ and *Ri* are not restricted. Application of the constraints to ensemble fingers produces constraint values in dynamically plausible ranges for all three constraints. Application to maximum growth produces dynamically plausible values only for $\langle Fr_{w/f}\rangle_m$.

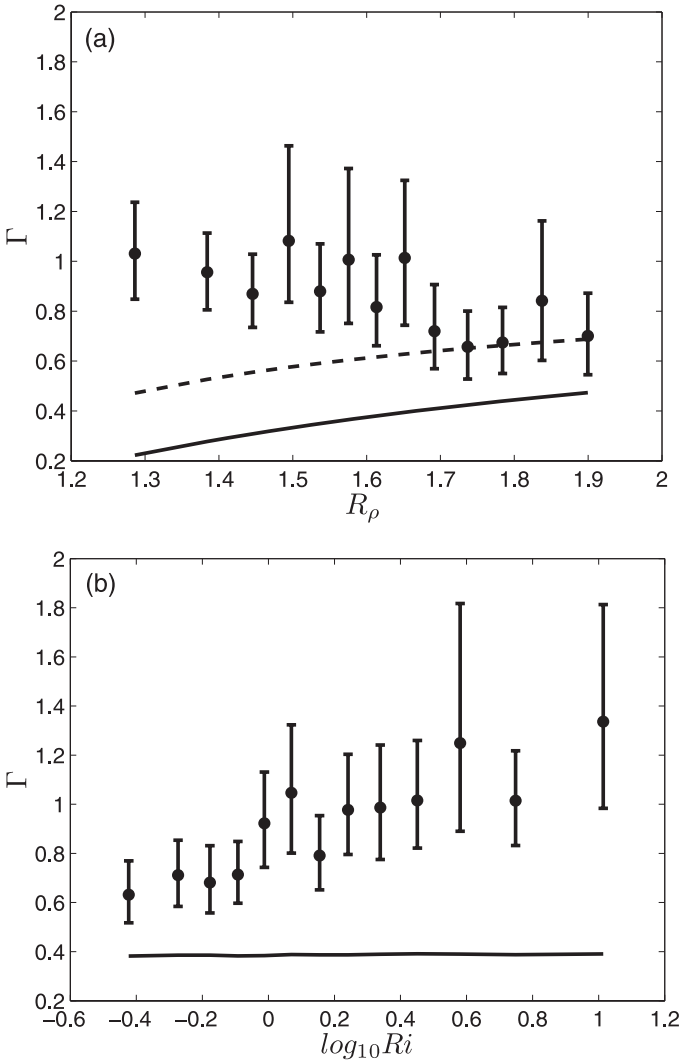

Figure 4. Average mixing efficiency Γ as a function of (a) density ratio R_ρ and (b) Richardson number *Ri*. Black circles are observed values, the solid line is for fastest-growing fingers from (7) and the dashed line in (a) is the Hamilton *et al.* (1989) relation. 95% confidence limits for theories are smaller than the line width. Parameterized values are estimated from averages described in Section 3.

Comparison of the R_ρ and *Ri* dependences of the observations and the model with the various constraints is shown in Figures 6 and 7. Although $Fr_{wf} \sim 1.5$ applied to ensemble fingers (solid red curves) reproduces observed *Re* and Cx_T in R_ρ space (thick black curves), the observations do not show the dependence on *Ri* predicted by the hybrid Froude number

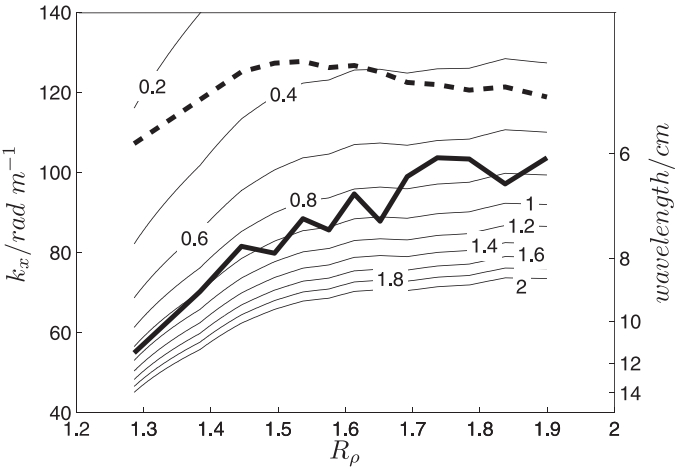

Figure 5. Fastest-growing (dashed) and best-fit (solid) wavenumbers as functions of density ratio R_ρ. Best-fit wavenumbers are obtained by matching observed and theoretical (6) mixing efficiencies Γ. The theoretical Γ from (6) is contoured for values of 0 to 2. The theoretical contours and fastest-growing curve for Γ are not smooth because observed $\bar{N}^2$ as a function of density ratio R_ρ (Fig. 3) are used.

constraint (Kunze, 1994). Likewise, although $Re_f \sim 1.7$ applied to ensemble fingers (solid blue curves) reproduces *Re* and Cx_T in *Ri* space, the predicted trend is opposite to that observed in R_ρ space. These results suggest that the $Fr_{w/f}$ and Re_f constraints are not appropriate. The trends of observed *Re* and Cx_T *can* be reproduced at all but the lowest resolved density ratio, $R_\rho = 1.3$, by $Ri_f \sim 0.2$ applied to ensemble fingers (solid green curves); *Re* and Cx_T at $R_\rho = 1.3$ are reproduced with $Ri_f = 0.15$. Cox numbers from an empirical fitting to a two-dimension numerical simulation by Stern *et al.* (2001)

$$Cx_{Stern} = 1.06\ \exp\left(\frac{5.62}{R_\rho}\right) \tag{16}$$

(solid pink curve, Fig. 7a) reproduce the observed trends and values, in particular as $R_\rho \to 1$.

Best-fit constraint values applied to *maximum* finger amplitudes that reproduce observed *Re* and Cx_T ($\langle\rangle_m$ in Table 2, dashed curves in Figs. 6-7) are either not consistent with dynamically plausible values or do not reproduce the observed dependence on R_ρ or *Ri*. This explains the discrepancy with the magnitudes of the salt diffusivity inferred by St. Laurent and Schmitt (1999) since they based their parameterized estimates on maximum-amplitude fluxes. Kunze (1987) reproduced a subset of inferred fluxes in the thermohaline staircase east of Barbados applying the Ri_f constraint to maximum finger amplitudes. However, this was based on $Re \sim 2$ and $Cx_T \sim 8$ while $Re \sim 20$ and $Cx_T \sim 60$ appear to be more typical values (Gregg and Sanford, 1987).

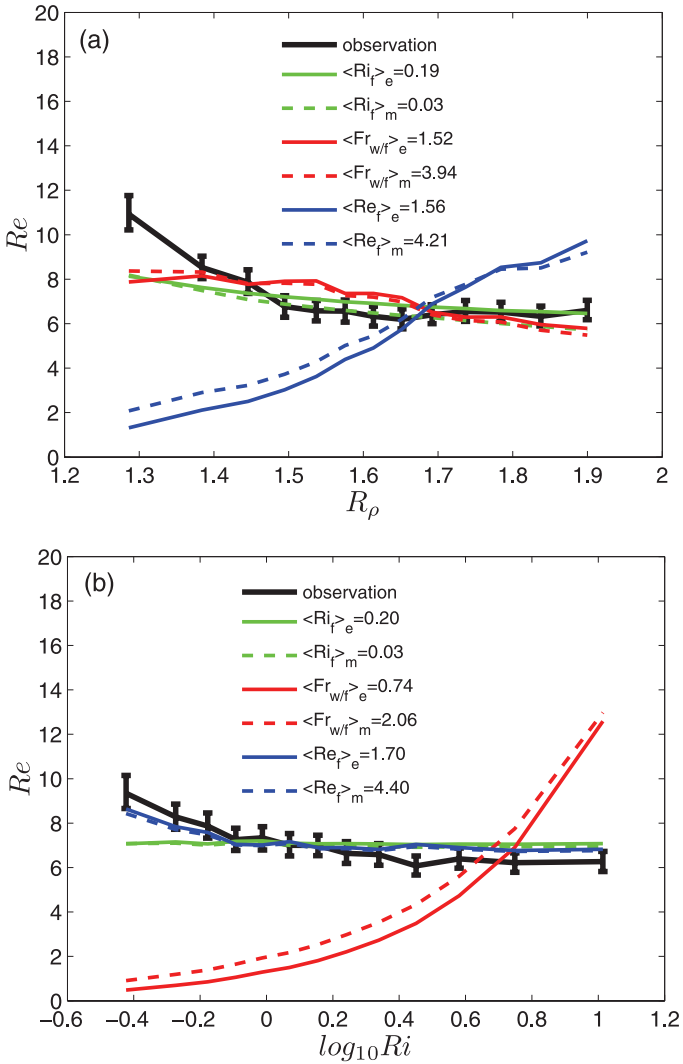

Figure 6. Average dependence of buoyancy Reynolds number *Re* on 5-m (a) density ratio R_ρ and (b) Richardson number *Ri*. Vertical bars denote 95% confidence limits. Angle brackets $\langle\rangle_e$ in the index corresponds to the constraints being applied to the ensemble-average best-fit fingers (Fig. 5), $\langle\rangle_m$ to their being applied to best-fit growing fingers at their maximum amplitude.

5. Relaxation of assumptions

Fastest-growing fingers (3), (4) and (7) can reproduce neither the level nor R_ρ dependence of the observed mixing efficiency Γ (Fig. 4). However, lower wavenumbers ($k < k_{FG}$) have theoretical mixing efficiencies consistent with the observations (6). Best-fit wavenumbers to the observed mixing efficiency Γ range from $0.5k_{FG}$ for $R_\rho = 1.3$ to

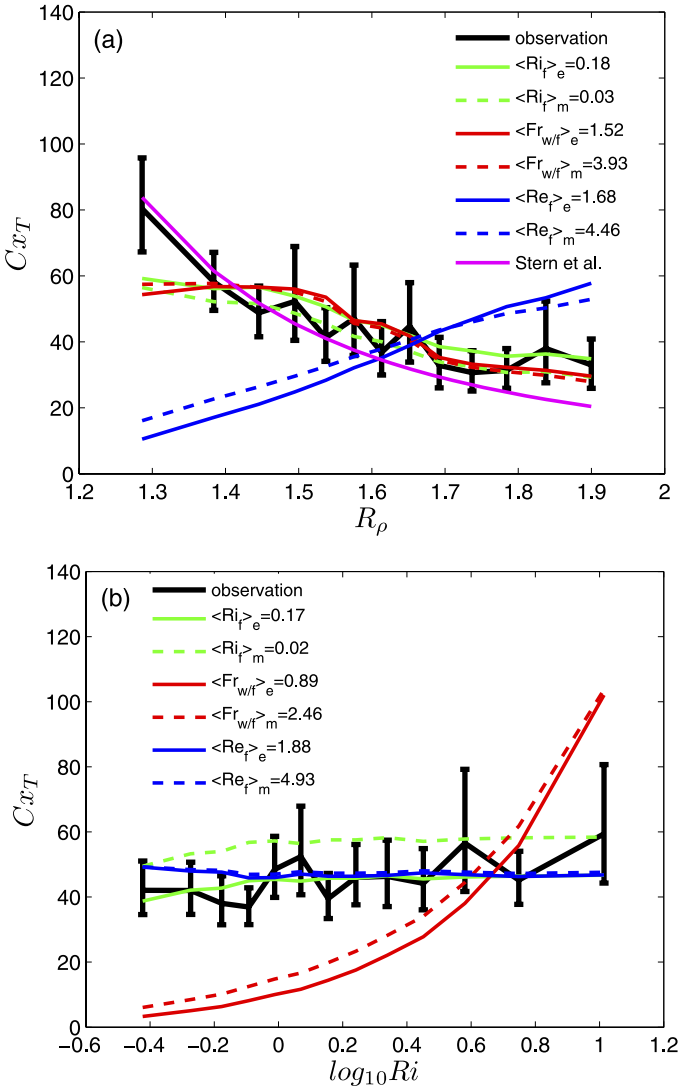

Figure 7. Average Cox number Cx_T as a function of (a) density ratio R_ρ and (b) Richardson number Ri. The index is as in Figure 6. The pink solid line in (a) is from numerical simulations by Stern *et al.* (2001). Vertical bars denote 95% confidence limits.

$0.9k_{FG}$ for $R_\rho = 2$ (Fig. 5). When ensemble-average finger amplitudes $\langle h \rangle_e$ for these wavenumbers are constrained with a dynamically plausible value of the finger Richardson number $Ri_f \sim 0.2$, linear theory is able to reproduce the observed Re and Cx_T at all but the lowest density ratio of $R_\rho = 1.3$ (Figs. 6-7).

The fact that Cx_T from Stern *et al.* (2001) better matches the observed R_ρ trends at low R_ρ

Table 2. Constraint values for Re (Fig. 6) and Cx_T (Fig. 7). Numbers in angle brackets $\langle\rangle_e$ correspond to the constraints being applied to best-fit (Fig. 5) ensemble-average Re and Cx_T from (6). Those in $\langle\rangle_m$ correspond to the constraints being applied to maximum values of best-fit growing fingers which then are normalized by (15). Bold numbers are close to dynamically plausible values (within 60% of $Ri_f = 0.25$, $Fr_{w/f} = 2.0$ and $Re_f = 1.0$).

constraints for Re	R_ρ space (Fig. 6a)	Ri space (Fig. 6b)
$\langle Ri_f\rangle_e\ \langle Ri_f\rangle_m$	$\langle\mathbf{0.19}\rangle_e\ \langle 0.03\rangle_m$	$\langle\mathbf{0.20}\rangle_e\ \langle 0.03\rangle_m$
$\langle Fr_{w/f}\rangle_e\ \langle Fr_{w/f}\rangle_m$	$\langle\mathbf{1.52}\rangle_e\ \langle 3.94\rangle_m$	$\langle 0.74\rangle_e\ \langle\mathbf{2.06}\rangle_m$
$\langle Re_f\rangle_e\ \langle Re_f\rangle_m$	$\langle\mathbf{1.56}\rangle_e\ \langle 4.21\rangle_m$	$\langle 1.70\rangle_e\ \langle 4.40\rangle_m$
constraints for Cx_T	R_ρ space (Fig. 7a)	Ri space (Fig. 7b)
$\langle Ri_f\rangle_e\ \langle Ri_f\rangle_m$	$\langle\mathbf{0.18}\rangle_e\ \langle 0.03\rangle_m$	$\langle\mathbf{0.17}\rangle_e\ \langle 0.02\rangle_m$
$\langle Fr_{w/f}\rangle_e\ \langle Fr_{w/f}\rangle_m$	$\langle\mathbf{1.52}\rangle_e\ \langle 3.93\rangle_m$	$\langle\mathbf{0.89}\rangle_e\ \langle\mathbf{2.46}\rangle_m$
$\langle Re_f\rangle_e\ \langle Re_f\rangle_m$	$\langle 1.68\rangle_e\ \langle 4.46\rangle_m$	$\langle 1.88\rangle_e\ \langle 4.93\rangle_m$

(Fig. 7) suggests that some physics may be missing in the assumptions used for the finger model that might explain the observed behavior at $R_\rho = 1.3$. Here, several of these assumptions will be separately relaxed to examine their impact. We will assume that a single constant $Ri_f \sim 0.2$ for ensemble-average fingers constrains finger growth based on Figures 6-7. First, we verify viscous control ($\nu\nabla^2 \gg \partial/\partial t$). Second, a salt-finger wavenumber spectral model (Schmitt, 1979a; Shen and Schmitt, 1995) is used to estimate contributions from wavenumbers other than best-fit wavenumbers. Finally, a simple model is developed to relax the assumption of tall-narrow fingers ($\nabla^2 \approx \partial^2/\partial x^2 + \partial^2/\partial y^2$). Considering nonlinear advection in the momentum and scalar equations is beyond the scope of our study. We only revisit trends of Re and Cx_T in R_ρ space because the observations show little Ri dependence (Figs. 6-7).

a. Viscous damping

For the vertical momentum equation (1), we followed standard practice and neglected vertical acceleration $\partial w/\partial t$ which is much smaller than the viscous term $\nu\nabla^2 w$ for all but $R_\rho \to 1$ (Schmitt, 1979a; Smyth and Kimura, 2007). Relaxing this viscous damping control, the time rate of change term $\partial w/\partial t$ will have the same sign as the viscous term $-\nu\nabla^2 w$. Thus, for a given w, one would need a larger buoyancy term $b = g(\alpha\delta\theta - \beta\delta S)$. This implies larger $\delta\theta$ and δS anomalies as well as larger property fluxes and thermal Cox numbers. Here, rather than solve the full cubic problem for σ and k^2, we formulate an ad-hoc amplification factor $(\nu k^2 + \sigma)/\nu k^2$ (Fig. 8) which reflects how much larger the buoyancy b would have to be if vertical acceleration were included. Approximating the growth rate $\sigma(k)$ from (2) for best-fit wavenumbers k, that is, neglecting vertical acceleration and using averaged background values (e.g., $\beta\bar{S}_z$), the amplification might enhance Cox numbers Cx_T, the buoyancy b and buoyancy-fluxes wb as $R_\rho \to 1$ (Fig. 8); amplification is larger for best-fit than fastest-growing wavenumbers. However, since Re

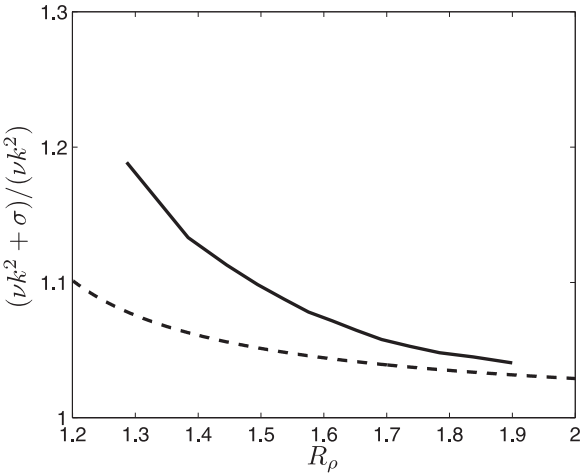

Figure 8. Amplification factor $(\nu k^2 + \sigma)/(\nu k^2)$ for buoyancy b if acceleration term $\partial w/\partial t$ is included in vertical momentum conservation (1). The solid line is for best-fit wavenumbers (Fig. 5) and dotted line for fastest-growing wavenumbers $k_{\rm FG}$ from (3) and (4).

and Ri_f scale in the same way (6), relaxing viscous control does not impact Re (Fig. 6). A more rigorous analysis that solves the full cubic finds a less than 3% change in the growth rate $\sigma(k)$ at $R_\rho = 1.3$ and no improvement in replicating the observed Re and Cx_T at low density ratio.

b. Contributions from other wavebands

Another possible explanation for the difference between observed and predicted Re and Cx_T as density ratio R_ρ approaches 1 may arise from contributions by other than best-fit wavenumbers. To explore this possibility, we use a spectral model (Schmitt, 1979a; Shen and Schmitt, 1995) based on linear growth theory (1) and propose a scenario in which salt-finger growth is disrupted by the finger Richardson number criterion (8). This approach requires a seed spectrum

$$\int_{k_0}^{k_1} S[w_0](k)dk = \langle w_0^2 \rangle, \tag{17}$$

where $S[w_0](k)$ is the horizontal wavenumber spectra for vertical velocity w and k_0 the lower bound of the integration which is set arbitrarily to be the wavenumber below $k_{\rm FG}$ in (4) for which the growth rate $\sigma(k_0) = \sigma_{\rm FG}/10$, approximately

$$k_0^2 = \frac{1}{10}\sqrt{\frac{g\beta\bar{S}_z}{\nu\kappa_T}}\,(R_\rho - 1)(\sqrt{R_\rho} - \sqrt{R_\rho - 1}). \tag{18}$$

k_1 is the upper bound of the integration, set to the wavenumber for steady fingers

$$k_1^2 \cong \sqrt{\frac{g\beta\bar{S}_z R_\rho}{\nu\kappa_S}}. \tag{19}$$

The seed variance $\langle {w_0}^2 \rangle$ is chosen arbitrarily to be $O[(w_{max}/100)^2] \sim 10^{-12}$ m^2 s^{-2} so will depend on finescale parameters $g\beta\bar{S}_z$ and R_ρ. Assuming power spectra of the form k^n and $k_1 \gg k_0$, we can express the seed spectra as

$$S[w_0](k) = \frac{(n+1)\langle w_0^2 \rangle}{k_1^{n+1}} k^n \quad \text{for } n \geq 0 \tag{20}$$

$$S[w_0](k) = \frac{(n+1)\langle w_0^2 \rangle}{k_0^{n+1}} k^n \quad \text{for } n \leq -2 \tag{21}$$

to recover $\langle w_0^2 \rangle$ upon integration (17). This approach will not work for a k^{-1} spectrum ($n = -1$). As fingers grow, the spectra evolves as

$$S[w](k) = S[w_0](k)\exp[2\sigma(k)t] \tag{22}$$

with different wavenumbers k growing at different rates $\sigma(k)$ (2).

For the finger Richardson number constraint, the goal is to find the time t_{max} such that

$$\begin{aligned} \int_{k_0}^{k_1} S[Ri_f^{-1}](k)dk &= \frac{C_w}{N_f^2}\int_{k_0}^{k_1} k^2 S[w](k)dk \\ = \frac{C_w}{N_f^2}\int_{k_0}^{k_1} k^2 S[w_0](k)\exp[2\sigma(k)t_{max}]dk &= Ri_{fcr}^{-1}. \end{aligned} \tag{23}$$

This constraint weights higher wavenumbers. For this reason, best-fit wavenumbers in Figure 5 are increasing functions of R_ρ. We note that the inverse finger Richardson number Ri_f^{-1} is used in this expression. We use critical values for Ri_f from Table 2.

Microscale buoyancy Reynolds number Re and thermal Cox number Cx_T can be written spectrally as

$$\begin{aligned} Re &= \frac{C_w}{\bar{N}^2}\int_{k_0}^{k_1} k^2 S[w](k)dk, \\ Cx_T &= C_T \int_{k_0}^{k_1} \frac{k^2 S[w](k)}{[2\sigma(k) + \kappa_T k^2]^2}\, dk. \end{aligned} \tag{24}$$

Because $Re = N_f^2/(Ri_f \bar{N}^2)$ (8), Re will be unchanged from Section 4 (Fig. 6). Cx_T is smaller and an increasing function of R_ρ because of its dependence on k (Fig. 9). Contributions from higher wavenumbers with faster growth rates contribute significantly. Therefore, fingers are arrested before Cx_T can become as large as in the single-

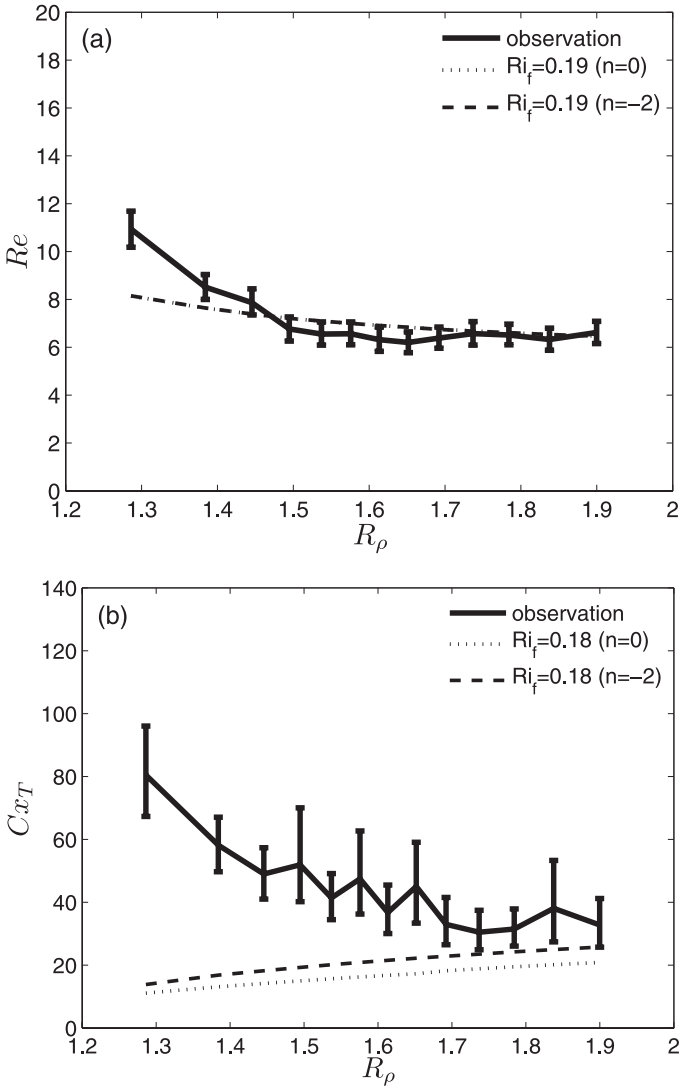

Figure 9. Average (a) microscale buoyancy Reynolds number *Re* and (b) Cox number Cx_T as functions of density ratio R_ρ from the spectral finger model. The dotted lines use seed spectrum (20), the dashed seed spectrum (21). Vertical axes ranges were chosen to correspond to those of Figures 6 and 7.

wavenumber case. Different seed spectral shapes have different impacts on Cx_T because Ri_f weights higher wavenumbers. Thus, $t_{\max}$ and Cx_T are larger when spectral slope $n \leq -2$ (21) (Fig. 9). The spectral approach could only reproduce the observed trends of Cx_T and Γ for a red seed spectrum which emphasizes $k \ll k_{\mathrm{FG}}$, meaning that contributions from low

wavenumbers dominate. This is commensurate with the best-fit wavenumbers being lower than fastest-growing wavenumbers (Fig. 5) so is not discussed further.

c. Short fingers

In obtaining the best-fit wavenumbers, tall narrow fingers ($\nabla^2 \approx \partial^2/\partial x^2 + \partial^2/\partial y^2$) are assumed. However, at low density ratios, growth is disrupted while fingers are still relatively short. This effect may be even more significant when finger wavenumbers are lower (Fig. 5). Here, we treat this possibility with a simple model assuming (i) viscous control and (ii) sinusoidal spatial structure [$\sin(k_x x)\sin(k_z z)$ where k_x and k_z are horizontal and vertical wavenumbers, respectively]. Then (1) can be rewritten

$$\begin{aligned} w &= \frac{g(\alpha\delta\theta - \beta\delta S)}{\nu k^2} \\ \frac{\partial(\alpha\delta\theta)}{\partial t} &= -\kappa_T k^2(\alpha\delta\theta) - w\alpha\theta_z \\ \frac{\partial(\beta\delta S)}{\partial t} &= -\kappa_S k^2(\beta\delta S) - w\beta S_z \end{aligned} \tag{25}$$

where $k^2 = k_x^2 + k_z^2$, $k_z \sim 2\pi/h$ and $h = h_0 + 2\int_0^t w dt$. This model ignores possible contributions from pressure p and horizontal velocities (u, v) that are likely to arise at finger tips and thus be more important for short fingers. Best-fit wavenumbers are used for k_x. We set the initial condition $h_0 = 2\pi/k_x$ so $k_0^2 = 2k_x^2$. Since these equations include terms that are nonlinear in k^2, $\kappa_T k^2 \alpha\delta\theta$ and $\kappa_S k^2 \beta\delta S$, these are integrated numerically with iteration. We assume that finger growth is arrested by threshold finger Richardson number Ri_f values from Table 2.

Re and Cx_T are estimated numerically setting $\partial w/\partial z \neq 0$ and $\partial\theta/\partial z \neq 0$

$$Re = \frac{C_w(k_x^2 + k_z^2)w^2}{\bar{N}^2}, \quad Cx_T = \frac{C_T(k_x^2 + k_z^2)(\delta\theta)^2}{\bar{\theta}_z^2} \tag{26}$$

from (25) because growth rate σ becomes a function of time as h and hence total wavenumber k evolve. Re and Cx_T estimated from the short-finger model (Fig. 10) produce almost the same results as the tall narrow fingers of Section 4 (Figs. 6-7) because fingers become sufficiently tall before they become unstable that the vertical structure does not matter. Thus, relaxing the tall-narrow finger assumption does not significantly modify fluxes.

6. Summary and discussion

A subset ($Ri > 0.25$, $1 < R_\rho < 2$, $Re < 20$) of the NATRE fine- and microstructure data set (St. Laurent and Schmitt, 1999) was revisited to test theories for salt-finger amplitude. These data are characterized by dissipation rates $\varepsilon = 5 \times 10^{-11}$ to 5×10^{-9} W kg^{-1}

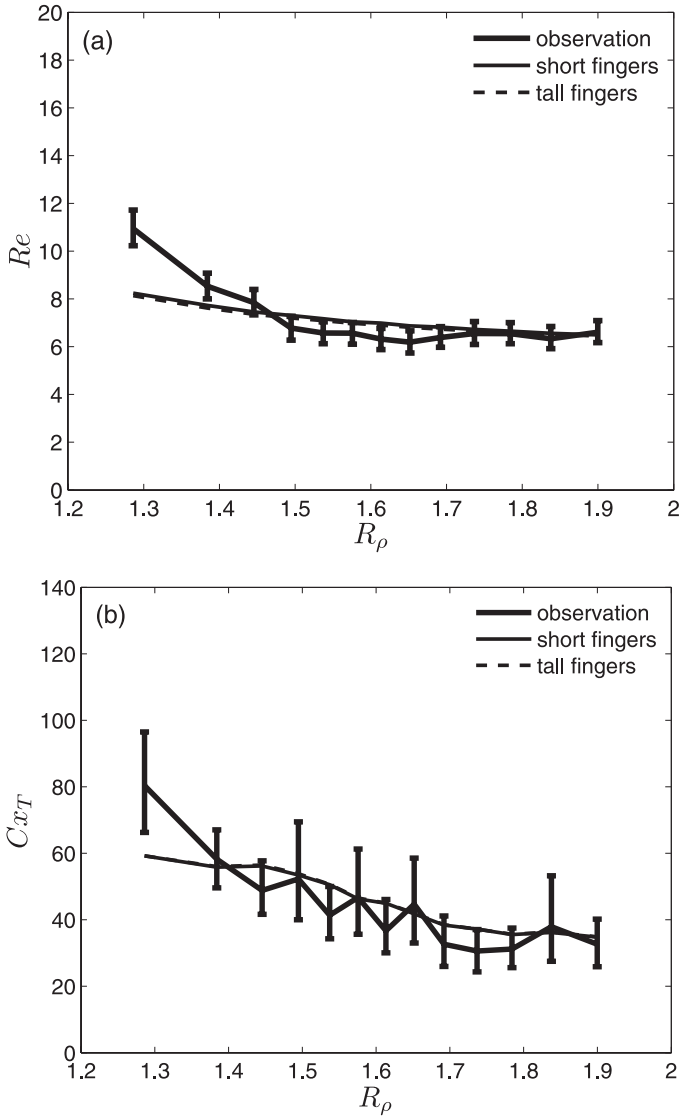

Figure 10. Average (a) microscale buoyancy Reynolds number *Re* and (b) Cox number Cx_T as a function of density ratio R_ρ from the short-finger model (dashed curve). Vertical axes ranges were chosen to correspond to those of Figures 6 and 7. Short (thin solid curve) and long (dashed curve) finger results are indistinguishable.

(Fig. 1). Observed microscale buoyancy Reynolds numbers Re decrease with increasing density ratio R_ρ and Richardson number *Ri* (Fig. 6). Observed thermal Cox numbers Cx_T decrease with increasing R_ρ (Fig. 7).

Observed mixing efficiencies Γ decrease with increasing R_ρ and increase with *Ri*

(Fig. 4). The trend with Ri might be attributed to low-Reynolds-number turbulence at low Ri. However, observed mixing efficiencies Γ are too high and have the wrong trends in R_ρ to be explained by either turbulence or linear fastest-growing fingers (Fig. 4). Linear fingers with wavenumbers lower than fastest-growing can have similar mixing efficiencies (6). Finger wavenumbers that reproduce the observed Γ range from $0.5k_{FG}$ at $R_\rho = 1.3$ to $0.9k_{FG}$ at $R_\rho = 2$ (Fig. 5).

Assuming best-fit wave numbers and applying three ad-hoc instability constraints to the average finger amplitude (finger Richardson number Ri_f, hybrid wave/finger Froude number $Fr_{w/f}$ and finger Reynolds number Re_f), it is shown that a dynamically plausible critical $Ri_f \sim 0.2$ (Kunze, 1987) can reproduce the average Re and Cx_T level as well as their dependence on density ratio R_ρ and background Richardson number Ri at all but the lowest density ratio $R_\rho = 1.3$. $Ri_f \sim 0.2$ underestimates Re and Cx_T by roughly 30% as $R_\rho \rightarrow 1.3$. It also underestimates Re at the lowest resolved Richardson number $Ri \sim 0.4$ but not Cx_T which may indicate contamination by low-Reynolds number turbulence. The observed Cx_T dependence on R_ρ agrees with recent numerical simulation estimates (Stern *et al.*, 2001).

The $Fr_{w/f}$ constraint (Kunze, 1994) cannot reproduce observed trends with Ri. Re_f (this paper) cannot reproduce observed trends with R_ρ (Figs. 6-7). We conclude that neither the hybrid wave/finger Froude number $Fr_{w/f}$ nor finger Reynolds number Re_f are appropriate constraints on finger amplitude. The former refutes the suggestion of Kunze (1994) that background shear fundamentally changes the secondary instability of salt fingers. A better understanding of what controls secondary instability and the maximum amplitude of salt fingers is needed.

Assumptions of (i) viscous control ($\nu k^2 \gg \sigma$), (ii) single (best-fit) wavenumber and (iii) tall-narrow fingers ($\nabla^2 \approx k_x^2 + k_y^2$) were separately relaxed to see if they had any impact on the conclusions. Neither a spectral finger model (Fig. 9) nor relaxation of the tall-narrow finger approximation (Fig. 10) yield improved model fits to the data. Relaxation of viscous control (Fig. 8) would result in some amplification of the Cox numbers, buoyancy and buoyancy-fluxes at lower density ratio. However, since Re and Ri_f scale in the same way (8), relaxing this assumption does not impact Re so the fits in Figure 6 are not improved.

While this study has shown that linear salt fingers with amplitudes constrained by a dynamically plausible finger Richardson number $Ri_f \sim 0.2$ can reproduce much of the observations, this could only be achieved by choosing wavenumbers lower than fastest-growing to reproduce the observed mixing efficiency γ (which should be independent of finger amplitude). These best-fit wavenumbers ranged from $0.5k_{FG}$ at $R_\rho = 1.3$ to $0.9k_{FG}$ at $R_\rho = 2$. These were found in an ad-hoc manner by insisting that the theory reproduce observed mixing efficiencies Γ (Figs. 4 and 5). No general explanation is offered for why oceanic finger wavenumbers might be lower than fastest-growing. Observed horizontal wavenumber spectra (Gargett and Schmitt, 1982; Marmorino and Greenewalt, 1988) often show excess variance at wavenumbers below the peak as compared to a spectral model but these have proven difficult to interpret because the horizontal structure of fingers in the ocean has not been established; if salt sheets are present, lower apparent wavenumbers may

be present depending on the angle of attack. Fleury and Lueck (1992) found peak wavenumbers below fastest-growing in the interfaces of the thermohaline staircase east of Barbados but also reported lower-than-predicted dissipation rates. Taylor (1991) found lower wavenumbers in laboratory experiments following disruption by turbulence but fastest-growing scales dominated once the fingers had re-established a statistical steady state. In summary, conclusive observational support for lower wavenumbers dominating is absent.

An issue not treated here is that temperature microstructure must cascade to higher wavenumbers than momentum in order to dissipate. If the microscale wavenumbers for these two variables scale as $k_T/k_\nu = \sqrt{\nu/\kappa_T}$ (Batchelor, 1959), this will boost the mixing efficiency Γ by ν/κ_T. Moreover, the 2/5 isotropy factor (5) arguably should be applied to the theoretical as well as the observational estimates for consistency. Combining these two effects brings the average mixing efficiency for fastest-growing fingers into the observed range. However, the theoretical trend with density ratio is still in the reverse sense to that observed. Insisting again that the theoretical Γ reproduce that observed produces a second set of wavenumbers that range from slightly below fastest-growing at the lowest R_ρ to slightly above. Seeking a critical Ri_f that best explains the observations, one finds $\langle Ri_f \rangle_e = 0.95 \pm 0.02$ and $\langle Ri_f \rangle_m = 0.43 \pm 0.01$. In this case, the predicted Re and Cx_T exceed the observations at $R_\rho = 1.3$ and fall below them at $R_\rho > 1.7$. The difference in temperature and velocity dissipation scales should be explored with direct numerical simulations.

If we assume the lower wavenumbers are correct (Fig. 5), at $R_\rho = 1.3$, one might argue that, at inception, vertical and horizontal wavenumbers are the same ($k_z = k_h$) such that $k_{TOT} \approx k_{FG}$ and $k_x \approx 0.5 k_{FG}$ (Fig. 5). However, this argument cannot be applied at higher density ratios where the best-fit $k \neq 0.5 k_{FG}$. Alternatively, fingers may be aliased to lower wavenumber through interaction with vertical internal wave straining (Schmitt and Evans, 1978); Kunze (1990) showed that interaction with near-inertial shear will tend to cause finger wavenumbers to catastrophically increase so cannot explain our inferences. Nonlinear advection terms (e.g., Radko and Stern, 1999; Stern and Simeonov, 2004; Stern and Simeonov, 2005) ignored here may play an important role in salt-finger dynamics. Stern and Simeonov (2005) found that the secondary instability is a subharmonic of fastest-growing fingers and most active at low R_ρ. Higher mixing efficiencies might also arise from assumptions about isotropy in the vertical profile data that were not applied consistently to horizontal microstructure predicted by theory though we are somewhat encouraged by the close agreement of the observed Cx_T with 2-D numerical simulations (Stern *et al.*, 2001). Without horizontal microstructure measurements or more complete analysis of direct numerical simulations, this issue cannot be resolved. It would also be valuable if future numerical simulation papers described the dependence of observables on density ratio R_ρ in addition to Cox number Cx_T such as dissipation rate ε, Reynolds number Re, peak wavenumber k, mixing efficiency Γ and flux ratio R_F.

Ferrari and Polzin (2005) and Smith and Ferrari (2008) argue that χ_T is stirred down from the largescale water-mass gradient between the Mediterranean salt tongue and

Labrador Sea Water by geostrophic eddies. They showed that all the χ_T could be explained by this eddy stirring on isopycnals occupied by these two water-masses. In this scenario, the mixing efficiency Γ is largely a combination of χ_T from lateral eddy stirring and dissipation rate ε from isotropic turbulence associated with diapycnal mixing. If the eddy-stirring mechanism holds, lateral processes and not salt-fingering dynamics would control χ_T and Γ so these variables would not illuminate salt-finger processes. However, the depth range where this interleaving occurs has $R_\rho > 2$ and is below that included in the data subset examined here where the *T-S* curve is relatively tight so that stirring-induced interleaving seems less likely.

Acknowledgments. The authors benefited from discussions with Timour Radko and Raf Ferrari. Comments from an anonymous reviewer improved the manuscript. We gratefully acknowledge the support of the Office of Naval Research (grant N00014-04-1-0212) and Natural Sciences and Engineering Research Council of Canada.

REFERENCES

Batchelor, G. K. 1959. Small-scale variation of convected quantities like temperature in turbulent fluid: I, General discussion and the case of small conductivity. J. Fluid Mech., *55*, 113-133.

Efron, B. and G. Gong. 1983. A leisurely look at the bootstrap, the jacknife and cross-validation. Amer. Stat., *37*, 36-48.

Ferrari, R. and K. L. Polzin. 2005. Finescale structure of the *T-S* relation in the eastern North Atlantic. J. Phys. Oceanogr., *35*, 1437-1454.

Fleury, M. and R. G. Lueck. 1991. Fluxes across a thermohaline interface. Deep-Sea Res., *38*, 745-769.

—— 1992. Microstructure in and around a double-diffusive interface. J. Phys. Oceanogr., *22*, 701-718.

Gargett, A. E. 1988. The scaling of turbulence in the presence of stable stratification. J. Geophys. Res., *93*, 5021-5036.

Gargett, A. E. and R. W. Schmitt. 1982. Observations of salt fingers in the Central Waters of the eastern North Pacific. J. Geophys. Res., *87*, 8017-8029.

Gregg, M. C. 1988. Mixing in the thermohaline staircase east of Barbados, *in* Small-Scale Turbulence and Mixing in the Ocean, J. C. J. Nihoul and B. M. Jamart, eds., Elsevier Oceanogr. Ser., *46*, 453-470.

Gregg, M. C. and T. B. Sanford. 1987. Shear and turbulence in thermohaline staircases. Deep-Sea Res., *34*, 1689-1696.

Griffiths, R. W. and B. R. Ruddick. 1980. Accurate fluxes across a salt-sugar finger interface deduced from direct density measurements. J. Fluid Mech., *99*, 85-95.

Hamilton, J., M. Lewis and B. R. Ruddick. 1989. Vertical fluxes of nitrate associated with salt fingers in the world's oceans. J. Geophys. Res., *94*, 2137-2145.

Hamilton, J., N. S. Oakey and D. E. Kelley. 1993. Salt-finger signatures in microstructure measurements. J. Geophys. Res., *98*, 2453-2460.

Hebert, D. 1988. Estimates of salt-finger fluxes. Deep-Sea Res., *35*, 1887-1901.

Holyer, J. Y. 1984. The stability of long, steady, two-dimensional salt fingers. J. Fluid Mech., *147*, 169–185.

Itsweire, E. C., K. N. Helland and C. W. Van Atta. 1986. The evolution of grid-generated turbulence in a stably stratified fluid. J. Fluid Mech., *162*, 299-338.

Kunze, E. 1987. Limits on growing finite-length salt fingers: A Richardson number constraint. J. Mar. Res., *45*, 533-556.

—— 1990. The evolution of salt fingers in inertial wave shear. J. Mar. Res., *48*, 471-504.
—— 1994. A proposed constraint for salt fingers in shear. J. Mar. Res., *52*, 999-1016.
—— 2003. A review of oceanic salt-fingering theory. Prog. Oceanogr., *56*, 399-417.
Kunze, E., A. J. Williams III and R. W. Schmitt. 1987. Optical microstructure in the thermohaline staircase east of Barbados. Deep-Sea Res., *34*, 1697-1704.
Lambert, R. B. and J. W. Demenkow. 1971. On the vertical transport due to fingers in double-diffusive convection. J. Fluid Mech., *54*, 627-640.
Lambert, R. B. and W. Sturges. 1977. A thermohaline staircase and vertical mixing in the thermocline. Deep-Sea Res., *24*, 211-222.
Ledwell, J. R., A. J. Watson and C. S. Law. 1993. Evidence for slow mixing across the pycnocline from an open-ocean tracer release experiment. Nature, *364*, 701-703.
Linden, P. F. 1971. Salt fingers in the presence of grid-generated turbulence. J. Fluid Mech., *49*, 611-624.
—— 1973. On the structure of salt fingers. Deep-Sea Res., *20*, 325-340.
—— 1974. Salt fingers in a steady shear flow. Geophys. Fluid Dyn., *6*, 1-27.
Lueck, R. G. 1987. Microstructure measurements in a thermohaline staircase. Deep-Sea Res., *34*, 1677-1688.
Magnell, B. 1976. Salt fingers observed in the Mediterranean outflow region (34°N, 11°W) using a towed sensor. J. Phys. Oceanogr., *6*, 511-523.
Marmorino, G. O. and D. Greenewalt. 1988. Inferring the nature of microstructure signals. J. Geophys. Res., *93*, 1219-1225.
McDougall, T. J. 1988. Some implications of ocean mixing on modeling, *in* Small Scale Turbulence and Mixing in the Ocean, J. C. J. Nihoul and B. M. Jamart, eds., Elsevier Oceanogr. Ser., *46*, 21-35.
McDougall, T. J. and J. R. Taylor. 1984. Flux measurements across a finger interface at low values of the stability ratio. J. Mar. Res., *42*, 1-14.
Merryfield, W. J. 2000. Origin of thermohaline staircases. J. Phys. Oceanogr., *30*, 1046-1068.
Oakey, N. S. 1982. Determination of the rate of dissipation of turbulent energy from simultaneous temperature and velocity shear microstructure measurements. J. Phys. Oceanogr., *12*, 256-271.
Osborn, T. R. 1980. Estimates of the local rate of vertical diffusion from dissipation measurements. J. Phys. Oceanogr., *10*, 83-89.
Osborn, T. R. and C. S. Cox. 1972. Oceanic finestructure. Geophys. Fluid Dyn., *3*, 321-345.
Özgökmen, T. M. and O. E. Esenkov. 1998. Asymmetric salt fingers induced by a nonlinear equation of state. Phys. Fluids, *10*, 1882-1890.
Özgökmen, T. M., O. E. Esenkov and D. B. Olson. 1998. A numerical study of layer formation due to fingers in double-diffusive convection in a vertically-bounded domain. J. Mar. Res., *56*, 463-487.
Piacsek, S.A., N.H. Brummell and B.E. McDonald. 1988. Numerical experiments on thermohaline convective motions across interfaces of intrusions, *in* Small Scale Turbulence and Mixing in the Ocean, J. C. J. Nihoul and B. M. Jamart, eds., Elsevier Oceanogr. Ser., *46*, 503-516.
Piacsek, S. A. and J. Toomre. 1980. Nonlinear evolution and structure of salt fingers, in Marine Turbulence, J. C. J. Nihoul, ed., Elsevier Oceanogr. Ser., *28*, 193-219.
Radko, T. 2003. A mechanism for layer formation in a double-diffusive fluid. J. Fluid Mech., *487*, 365-380.
—— 2005. What determines the thickness of layers in a thermohaline staircase? J. Fluid Mech., *523*, 79-98.
Radko, T. and M. E. Stern. 1999. Salt fingers in three dimensions. J. Mar. Res., *57*, 471-502.
—— 2000. Finite-amplitude salt fingers in a vertically bounded layer. J. Fluid Mech., *425*, 133-160.
Ruddick, B. R. and K. Richards. 2003. Oceanic thermohaline intrusions. Prog. Oceanogr., *56*, 499-527.

Ruddick, B., D. Walsh and N. Oakey. 1997. Variation in apparent mixing efficiency in the North Atlantic Central Water. J. Phys. Oceanogr., *27*, 2589-2605.

Schmitt, R. W. 1979a. The growth rate of supercritical salt fingers. Deep-Sea Res., *26A*, 23-44.

—— 1979b. Flux measurements at an interface. J. Mar. Res., *37*, 419-436.

—— 1981. Form of the temperature-salinity relationship in the Central Water: Evidence for double-diffusive mixing. J. Phys. Oceanogr., *11*, 1015-1026.

—— 2003. Observational and laboratory insights into salt finger convection. Prog. Oceanogr., *56*, 419-433.

Schmitt, R. W. and D. L. Evans. 1978. An estimate of the vertical mixing due to salt fingers based on observations in the North Atlantic Central Water. J. Geophys. Res., *83*, 2913-2919.

Schmitt, R. W., J. R. Ledwell, E. T. Montgomery, K. L. Polzin and J. M. Toole. 2005. Enhanced diapycnal mixing by salt fingers in the thermocline of the tropical Atlantic. Science, *308*, 685-688.

Schmitt, R. W., J. M. Toole, R. L. Koehler, E. C. Mellinger and K. W. Doherty. 1988. The development of a fine- and microstructure profiler. J. Atmos. Oceanic Tech., *5*, 484-500.

Shen, C. Y. 1989. The evolution of the double-diffusive instability: Salt fingers. Phys. Fluids, *1*, 829-844.

—— 1993. Heat-salt finger fluxes across a density interface. Phys. Fluids, *5*, 2633-2643.

—— 1995. Equilibrium salt-fingering convection. Phys. Fluids, *7*, 706-717.

Shen, C. Y. and R.W. Schmitt. 1995. The wavenumber spectrum of salt fingers, *in* Double-Diffusive Convection, A. Brandt and H. Fernando, eds., AGU Geophysical Monograph *94*, 305-312.

Shen, C. Y. and G. Veronis. 1991. Scale transition of double-diffusive finger cells. Phys. Fluids, *3*, 58-68.

——1997. Numerical simulations of 2-D salt-fingers. J. Geophys. Res., *102*, 23,131-23,143.

Smith, K. S. and R. Ferrari. 2008. The production and dissipation of compensated thermohaline variance by mesoscale stirring. J. Phys. Oceanogr., (submitted).

Smyth, W. D. and S. Kimura. 2007. Instability and diapycnal momentum transport in a double-diffusive, stratified shear layer. J. Phys. Oceanogr., *37*, 1551-1565.

Stern, M. E. 1960. The "salt-fountain" and thermohaline convection. Tellus, *12*, 172-175.

—— 1969. Collective instability of salt fingers. J. Fluid Mech., *35*, 209-218.

—— 1975. Ocean Circulation Physics, Academic Press, New York, 246 pp.

Stern, M. E. and T. Radko. 1998. The salt-finger amplitude in unbounded *T-S* gradient layers. J. Mar. Res., *56*, 157-196.

Stern, M. E., T. Radko and J. Simeonov. 2001. Salt fingers in an unbounded thermocline. J. Mar. Res., *59*, 355-390.

Stern, M. E. and J. A. Simeonov. 2002. Internal wave overturns produced by salt fingers. J. Phys. Oceanogr., *32*, 3638-3656.

—— 2004. Amplitude equilibration of sugar-salt fingers. J. Fluid Mech., *508*, 265-286.

—— 2005. The secondary instability of salt fingers. J. Fluid Mech., *533*, 361-380.

Stillinger, D. C., K. N. Helland and C. W. van Atta. 1983. Experiments on the transition of homogeneous turbulence to internal waves in a stratified fluid. J. Fluid Mech., *131*, 91-122.

St. Laurent, L. and R. W. Schmitt. 1999. The contribution of salt fingers to vertical mixing in the North Atlantic tracer-release experiment. J. Phys. Oceanogr., *29*, 1404-1424.

Taylor, J. 1991. Laboratory experiments on the formation of salt fingers after the decay of turbulence. J. Geophys. Res., *96*, 12,497-12,510.

Taylor, J. and P. Bucens. 1989. Laboratory experiments on the structure of salt fingers. Deep-Sea Res., *36*, 1675-1704.

Toole, J. M. and D. T. Georgi. 1981. On the dynamics and effects of double-diffusively driven intrusion. Prog. Oceanogr., *10*, 121-145.

Toole, J. M., K. L. Polzin and R. W. Schmitt. 1994. Estimates of diapycnal mixing in the abyssal ocean. Science, *264*, 1120-1123.

Turner, J. S. 1967. Salt fingers across a density interface. Deep-Sea Res., *14*, 599-611.

Wells, M. G. and R. W. Griffiths. 2002. Localized stirring in a field of salt fingers. Dyn. Atmos. Oceans, *35*, 327-350.

Whitfield, D. W. A., G. Holloway, and J. Y. Holyer. 1989. Spectral transform simulations of finite amplitude double-diffusive instabilities in two dimensions. J. Mar. Res., *47*, 241-265.

Williams, A. J. 1974. Salt fingers observed in the Mediterranean outflow. Science, *185*, 941-943.

Winters, K. B. and J. J. Riley. 1992. Instability of internal waves near a critical level. Dyn. Atmos. Oceans, *16*, 249-278.

Yoshida, J. and H. Nagashima. 2003. Numerical experiments on salt-finger convection. Prog. Oceanogr., *56*, 435-459.

You, Y. 2002. A global ocean climatological atlas of the Turner angle: Implications for double diffusion and water-mass structure. Deep-Sea Res., *49*, 2075-2093.

Received: *20 March, 2008;* revised: *8 September, 2008.*